CrossMark

ORIGINAL PAPER

Evidence for Room-Temperature Weak Ferromagnetic and Ferroelectric Ordering in Magnetoelectric Pb(Fe$_{0.634}$W$_{0.266}$Nb$_{0.1}$)O$_3$ Ceramic

Shidaling Matteppanavar[1] · Shivaraja I[1] · Sudhindra Rayaprol[2] ·
Basavaraj Angadi[1] · Balaram Sahoo[3]

Abstract We report the evidence of weak ferromagnetic and ferroelectric ordering in polycrystalline Pb(Fe$_{0.634}$W$_{0.266}$Nb$_{0.1}$)O$_3$ (0.8(PbFe$_{2/3}$W$_{1/3}$)O$_3$–0.2Pb(Fe$_{1/2}$Nb$_{1/2}$)O$_3$) (PFWN) ceramic at room temperature. The Pb(Fe$_{0.634}$W$_{0.266}$Nb$_{0.1}$)O$_3$ solid solution synthesized through the columbite method. The obtained single-phase Pb(Fe$_{0.634}$W$_{0.266}$Nb$_{0.1}$)O$_3$ ceramic was subjected to X-ray diffraction, neutron diffraction, magnetization, Mössbauer spectroscopy, and ferroelectric measurements. The X-ray diffraction and neutron diffraction pattern confirms the formation of single phase without any traces of pyrochlore phases, having *cubic* structure with *Pm-3m* space group. The Rietveld refinements were carried out on both patterns, and ND data confirms the *G*-type antiferromagnetic structure with propagation vector ($k = 1/2, 1/2,$ and $1/2$). However, along with the antiferromagnetic ordering of the Fe spins, we also observed the existence of weak ferromagnetism. This result was confirmed through (i) a clear opening of hysteresis ($M - H$) loop, (ii) bifurcation of the field-cooled (FC) and zero-field-cooled (ZFC) susceptibilities, (iii) spin-glass behavior, and (iv) Mössbauer spectroscopy.

✉ Basavaraj Angadi
brangadi@gmail.com

[1] Department of Physics, Bangalore University, Jnanabharathi Campus, Bangalore, 560056, India

[2] UGC-DAE-Consortium for Scientific Research, Mumbai Centre, BARC Campus, Mumbai, 400085, India

[3] Materials Research Centre, Indian Institute of Science, Bangalore, 560012, India

1 Introduction

Pb-based multiferroics [1–3] are promising candidates for the design and synthesis of multifunctional materials. They are important for their unique and strong coupling of electric, magnetic, and structural order parameters, giving rise to simultaneous ferroelectricity, ferromagnetism, and ferroelasticity [4]. This is of great interest to study these compounds from a fundamental perspective, as well as for potential applications in magnetoelectric and magnetoelastic devices. In these systems, the interplay and competitions between spins, dopant charge carriers, the degree of freedom of orbital, and lattice symmetry lead to a variety of couplings and phase transitions [4]. Currently, most of the research on single-phase multiferroics is concentrated on lowering sintering temperatures as much as possible, without much change in the properties of the materials.

Among them, lead iron tungstate—Pb(Fe$_{2/3}$W$_{1/3}$)O$_3$ (PFW) and lead iron niobate—Pb(Fe$_{1/2}$Nb$_{1/2}$)O$_3$ (PFN) are widely studied multiferroic properties independently because of their unique multiferroic proprieties [5–7]. The PFW is known as a multiferroic material with a complex perovskite-type structure (AB′B″O$_3$) in which Fe^{3+} and W^{6+} are randomly distributed at the octahedral B-site positions and presents a relaxor ferroelectric and antiferromagnetic ordering. The ferroelectric Curie temperature (T_C) was reported to occur between 150 and 200 K [5]. PFN undergoes a normal ferroelectric phase transition which occurs around 380 K and an antiferromagnetic phase transition at 155 K [6, 7]. Unfortunately, these materials suffer

from high leakage current, formation of multiphase structure, high dielectric loss, etc., which limit the materials to be used for fabrication of any suitable devices with better performance. In the last few decades, several attempts have been made to solve these problems by (i) synthesizing single-phase materials using various techniques, (ii) modifying chemical composition of the materials by suitable substitutions at the A/B atomic sites, and (iii) fabricating multicomponent composites, and encouraging results have been obtained.

Nowadays, exotic results has been carried out to understand the magnetoelectric, magnetoelastic, and piezoelectric coupling of solid solutions $Pb(Fe_{2/3}W_{1/3})O_3$–$(Pb(ZrTiO3))$, $Pb(Fe_{2/3}W_{1/3})O_3$–$PbTiO_3$, and $Pb(Fe_{2/3}W_{1/3}) O_3$–$BiFeO_3$ [8–17] in bulk and thin film. Recently, Kumar et al. reported enormous piezoelectric coupling effect in $Pb(Zr_{0.53}Ti_{0.47})O_3$/$Pb(Fe_{0.66}W_{0.33})O_3$ (PFW-PZT) solid solutions [8] and Lee et al. reported that $(PbZr_{0.57}Ti_{0.43}O_3)_{0.8}$–$(PbFe_{0.67}W_{0.33}O_3)_{0.2}$ thin-film solid solutions show the better multiferroic properties [9]. Kempa et al. reported on bulk PFW-PZT and confirmed absence of magnetically switched off polarization [10], and Pajic et al. reported the competing antiferromagnetism and local magnetic order in the bulk ceramic PZT-PFW multiferroic system: searching for the most promising ratio between PZT and PFW [11]. Dulkin et al. reported $(1 − x)$ $Pb(Fe_{2/3}W_{1/3})O_3$–$xPbTiO_3$ solid solutions studied and corrected previously obtained phase diagram for ceramic system [12]. Choudhary et al. reported relaxor characteristics of $Pb(Fe_{2/3}W_{1/3})O_3$–$BiFeO_3$ solid solution prepared by mechanosynthesis route and obtained dielectric studies [13], and recently, Puli et al. reported on quaternary Pb-based materials $(0.25(PbZr_{0.52}Ti_{0.48}O_3) + 0.25(PbFe_{0.5}Ta_{0.5}O_3) + 0.25(PbF_{0.67}W_{0.33}O_3) + 0.25(PbFe_{0.5}Nb_{0.5}O_3))$ (PZT-PFT-PFW-PFN) and observed good ferroelectric and diffused dielectric properties [14]. Lee et al. [15] have studied the PFW-PFN solid solution for the single phase formation and to enhance their properties for the multi layer ceramic capacitor (MLCC) applications and later on, Liou et al. reported on $Pb((Zn_{1/3}Nb_{2/3})_{0.6}(Fe_{2/3}W_{1/3})_{0.4})O_3$ and $Pb((Fe_{1/2}Nb_{1/2})_{0.7}(Fe_{2/3}W_{1/3})_{0.3})O_3$ $(0.7PFN − 0.3PFW)$ solid solutions independently without magnetic and electric properties [16]. Recently, Ivanov et al. thoroughly studied the $0.6(Pb(Fe_{2/3}W_{1/3})O_3 − 0.4(Pb(Fe_{1/2}Nb_{1/2})O_3))$ solid solution and reported existence of weak magnetoelectric coupling in particular solid solutions [17].

From all the above consequences, it is confirmed that PFW is an attractive candidate for magnetoelectric, magnetoelastic, and piezoelectric coupling phenomenon; so in this work, we selected $((Pb(Fe_{0.634}W_{0.266}Nb_{0.1})O_3)$ (PFWN)) solid solution. Further, synthesis of single-phase multiferroics is a difficult task, even with different chemical and solid-state routes due to the reason that PFW-PFN solid

solutions are less studied. In this study, we fabricated particularly PFWN solid solution to understand the structure and magnetic and electric behavior of the ceramic at room temperature (RT), and it was not studied earlier. Some controversies and inconsistent interpretations were proposed to describe the RT weak ferromagnetic ordering and structure in Pb-based systems, in such a way that their origins still remain unclear.

In this present work, single-phase PFWN ceramic powder were synthesized by Columbite method, and its RT crystallographic and antiferromagnetic (AFM) structure was characterized using X-ray diffraction (XRD) and neutron diffraction (ND) studies. To assess the weak ferromagnetism at RT, we have performed magnetization, Mössbauer spectroscopy, and polarization ($P − E$ loop) measurements. Furthermore, we report the origin of this weak ferromagnetic behavior at RT in PFWN.

2 Experimental

2.1 Sample Preparation and Characterization

Polycrystalline samples of PFWN were prepared by a Columbite method [5, 18] (solid-state reaction method), a relatively low-temperature sintering (> 850 °C) and using high-purity (99.9%) ingredients; PbO, Fe_2O_3, WO_3, and Nb_2O_5 (Sigma Aldrich and SD Fine, India) in a suitable stoichiometry. Firstly, the reagent Fe_2O_3, WO_3, and Nb_2O_5 powders were stochiometrically mixed with ethanol and crushed fine powders for 2 h by using agate mortar. The mixed Fe_2O_3, WO_3, and Nb_2O_5 were calcined at 1000 °C for 4 h. Subsequently, the stochiometric PbO (99.9%; SD Fine, India) and $FeWNbO_6$ were mixed and crushed in agate mortar for 2 h with 1 wt.% excess of PbO added. After drying, this slurry was calcined at 900 °C for 2 h, and sintering was carried out at 850 °C for 90 min in high purity alumina crucibles. The calcined fine powders were cold pressed into cylindrical pellets of 10 mm diameter and 1–2 mm of thickness at a pressure of 3 tonnes using a hydraulic press. Polyvinyl alcohol (PVA) was used as binder to prepare the pellets, which can be removed completely during sintering. Then the pellets were sintered at 1123 K for 1 h in Pb-rich environment muffle furnace.

Pb-based multiferroics are challenging materials to achieve single phase due to the formation of in situ secondary phases, such as pyrochlores, along with the perovskite phase. One of the reasons for the formation of pyrochlore phases is the evaporation of Pb above 850 °C during the sintering process. In order to avoid the formation of pyrochlore phase, Pb evaporation has to be controlled. To achieve this, we have created a Pb-rich closed environment during the sintering process. $PbZrO_3$ was used as a

Pb source inside the closed environment, which is sealed to control the Pb partial pressure. To check the phase formation of the polycrystalline PFWN, we used XRD measurement. The sintered ceramic powder were characterized by XRD (Phillips 1070) using Cu-Kα radiation (wavelength, $\lambda = 1.5406$ Å) to obtain the crystal structure. Neutron diffraction measurements were carried out on a focusing crystal-based powder diffractometer, available at UGC-DAE-CSR beam line in Dhruva reactor, BARC. Neutrons at wavelength 1.48 Å were used for the present study. Rietveld analysis were carried out on powder XRD and ND data using the Fullprof suite programs for crystallographic as well as for magnetic structure studies [19].

Magnetization studies were carried out on a vibrating sample magnetometer (VSM) attached to a physical property measurement system (Quantum Design PPMS). The $M - H$ loop of our PFWN sample measured at RT up to an applied field of 90 kOe. The zero field-cooled (ZFC) and field-cooled (FC) variations of magnetic susceptibility ($\chi = M - H$) with temperature for the PFWN sample, measured in a field of 500 Oe.

[57]Fe Mössbauer spectroscopy is one of the most efficient tools to investigate the local magnetic ordering, behavior, and oxidation state of the iron atoms in the matrix. Transmission Mössbauer spectrum was measured at RT by using a 57Co source (Rh matrix, $\sim$ 15 mCi) mounted on a constant acceleration Mössbauer drive from SEE Co., USA and a proportional counter. The spectrum is a Zeeman split six-line pattern, where the black dots represent the experimentally recorded data points and the solid line is the least square fit to the measured data. The spectrum recording time was about 1 week, but still the signal/noise ratio of the spectrum is low due to the electronic absorption of Pb and W. For the least square fitting of the Mössbauer spectrum, we used the computer program NORMOS written by Brand [20]. The ferroelectric ($P - E$) loop measurements were carried out at RT by ferroelectric loop ($P - E$) tracer (M/s Radiant Instruments, USA). Thin silver paste is applied on both sides (top and bottom) of the PFWN ceramic pellet as the electrodes. For RT, $P - E$ measurements, the samples were immersed in silicone oil to prevent the electric arcing, if any, at high applied voltages.

3 Results and Discussion

3.1 Crystal Structure: XRD and ND

The differential thermal analysis or thermogravimetric (DTA/TG) curve of the ceramic is shown in Fig. 1. The sample sintered at different high temperatures such as 1100, 1050, and 900 °C, whereas the sample shows evidence of the second phase, probably most commonly arising from
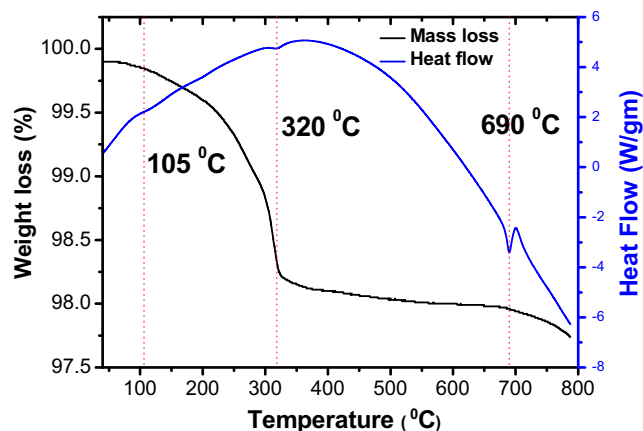

Fig. 1 Temperature dependence of weight loss and heat flow of PFWN measured by differential scanning calorimetry

Pb$_2$Nb$_2$O$_7$, PbWO$_4$, Pb$_2$W$_2$O$_7$, etc. and related pyrochlore phases. Hence, the rapid sintering at 850 °C shows a completion of reaction to form a single-phase PFWN solid solution. It is noted that the sintering temperature higher than that of 850 °C, such as at 1100, 1050, and 900 °C, forms many undesirable impurity phases. In order to investigate the thermal behavior related to phase changes and melting phenomena in PFWN solid solution, thermal gravimetric/differential thermal analysis (TG/DTA) results are presented in Fig. 1.

The differential thermal analysis or thermo gravimetric (DTA/TG) curve of the ceramic is shown in Fig. 1. Within the temperature range of 90–350 °C, a two-step decomposition of PbCO$_3$ to PbO (litharge) was observed. The decomposition was completed at 320 °C with distinct endothermic effects and a corresponding weight loss. A distinct endothermic transition at 690 °C in heat flow vs. temperature curve is observed. This transition is very consistent with the change in curvature in heat-flow curve and mass loss, as shown in Fig. 1 as dashed lines. The melting point of PbO is about 888 °C, and this transition can be certainly assigned due to the evaporation of PbO in the sample. On the other hand, there is a remarkable weight loss after the second transition at 690 °C, indicating loss of PbO through sublimation process. Hence, rapid heating rate and short-time sintering of PFWN at 850 °C remain as clues to avoid loss of PbO, segregation of Fe$_2$O$_3$, WO$_3$, and Nb$_2$O$_5$, and formation of other undesired phases such as pyrochlore phases.

Figure 2a shows the RT XRD pattern of PFWN ceramic prepared by Columbite solid state reaction method and sintered at 850 °C 1 h^{-1}, respectively. The Rietveld refinement analysis confirms that the sample forms in single-phase *cubic* structure (*Pm-3m* space group), with no secondary parasitic phases like Pb$_2$Nb$_2$O$_7$, PbWO$_4$, Pb$_2$W$_2$O$_7$, etc. [5, 18]. The structural parameters were obtained from the
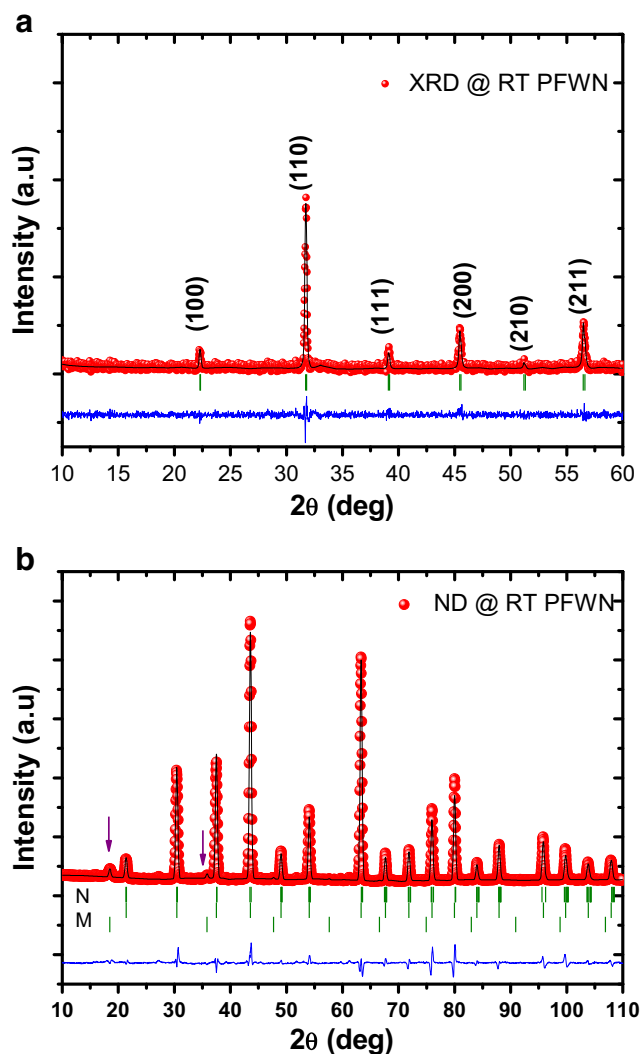
Fig. 2 **a** X-ray diffraction pattern and **b** neutron diffraction pattern of sintered PFWN sample. The observed data points are marked by (*red*) *circles*, whereas the *continuous lines passing through the data points* is the calculated profile. The (*blue*) *line at the bottom of the figure* indicates the difference between observed and calculated profiles. Bragg positions are marked by the *vertical* (*green*) *lines*. In (**b**), first row marked with *N* represents nuclear (crystallographic) Bragg peak positions and the second row marked with *M* represents magnetic Bragg peak positions

Rietveld refinement of the XRD data. The lattice parameter was found to be 3.987(1) Å. No additional superstructure peaks associated with the atomic ordering and tilting of the (Fe, W, Nb)O_6 perfect octahedra were detected. This suggests that the low-temperature calcination and sintering proved to be effective in achieving the single phase without any impurity phases. Good agreement was found between observed and calculated profiles for XRD data.

Further, more precise crystal structure of PFWN samples were determined from the Rietveld analysis of the RT ND data (Fig. 2b) and which further confirms the *cubic* structure with *Pm*-3*m* space group. In the Rietveld refinement,

the atoms were first fixed at their special positions, e.g., Pb cation was located at the position (000) (Wyckoff site 1a). The transition metal ions, Fe, W, and Nb are distributed randomly on crystallographic position given by the Wyckoff notation 1b, i.e., (1/2, 1/2, and 1/2), which is placed at half-cell apart from Pb. Oxygen is placed between Pb and Fe/W and forms a common face between Pb and Fe/W at Wyckoff site 3c, i.e., (1/2, 1/2, and 0). Figure 3a shows the crystallographic structure of PFWN drawn based on the refinement results of RT ND data. The Fe/W/Nb ratio of the B cation site was held constant during our refinements based on the results of the chemical analysis. The observed isotropic atomic displacement parameter of the lead (Pb) cation was obtained as unusually large (B_{Pb}). During the
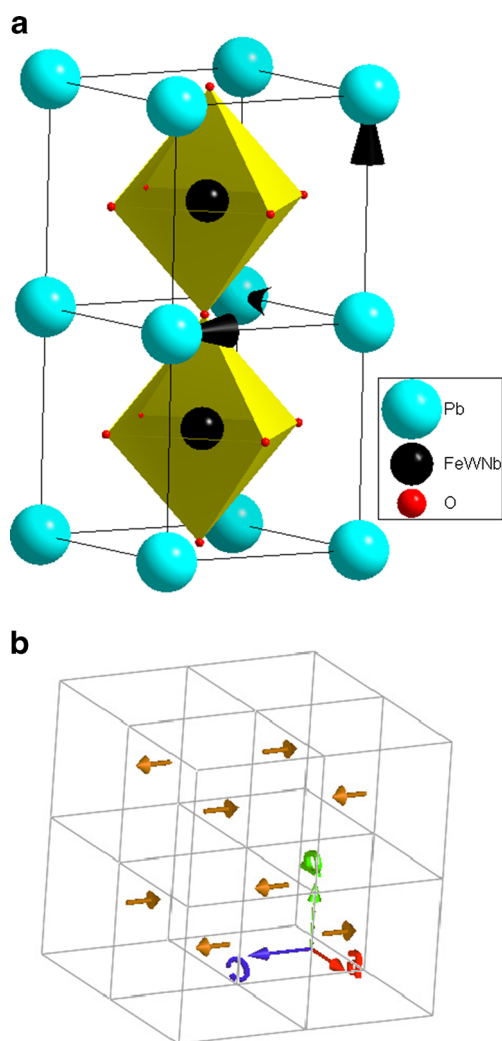

Fig. 3 **a** Crystal structure of PFWN. The lead atoms are located at the edges of the unit cell. Polyhedron is drawn around the iron, niobium/tungsten atoms. Oxygen atoms are shown in *red* (*at the edges of the polyhedra*). **b** Magnetic structure of PFWN. Only the moment on iron is shown as *arrows*. The *alternative arrangement of arrows* indicates the antiferromagnetic arrangement of magnetic ions, giving rise to the antiferromagnetic ordering at RT in PFWN

refinement, atomic occupancy of Pb was also refined for the PFWN sample to confirm the loss of Pb or O ions and variation within one standard deviation. The structural model used in refining the powder XRD data was taken as a starting model for the refinement of the ND data. The refined cell parameter from the analysis of RT ND data is $a = 3.988(1)$ Å, which is in good agreement with the XRD result ($a = 3.987(1)$ Å). The obtained R-factors ($R_p = 3.80\%; R_{wp} = 5.59\%; R_{exp} = 1.61\%; \chi^2 = 1.2$, Bragg R-factor = 3.76, Rf-factor = 1.74) are also found to be reasonably good [5, 7, 12, 17].

In Fig. 2b, the arrow marks clearly the extra Bragg peaks around 2θ (or Q^{-1}) of 18.5 2θ (1.36 Å^{-1}), 35.89θ (2.61 Å^{-1}), and 47.77θ (3.43 Å^{-1}), similar to the PFW and PFN [5, 17]. All these peaks could be identified as antiferromagnetic peaks and were indexed using a single propagation vector $k = (1/2, 1/2,$ and $1/2)$. For refinement, symmetry elements and basis vectors of the irreducible representations were obtained using BasIreps program within the Fullprof suite [21]. The magnetic phase was added as the second phase, and the refinement was carried out assuming Fe as the only magnetic ion in PFWN and obtained magnetic structure was a G-type antiferromagnetic structure. The value of the magnetic moment per Fe ion at RT is 5.5 μB, which is slightly lower than the calculated spin only value of 5.9 μB/Fe. The obtained R-factor for the magnetic phase (magnetic R-factor) is 16.2. Figure 3b shows that the Fe^{3+} moments are arranged in a simple G-type antiferromagnetic structure of PFWN as obtained from the Rietveld-refined ND pattern.

3.2 Magnetization Studies

The zero field cooling (ZFC) and field cooling (FC) temperature dependences of magnetization M(T) are shown in Fig. 4. For the sake of simplicity, this figure presents ZFC and FC data for 500 Oe of applied magnetic field only. To record the ZFC magnetization, the sample was first cooled to a low temperature in the absence of a magnetic field. Next, the magnetic field was applied and the ZFC measurements were performed on warming the sample. The FC data were also recorded on warming, after previous cooling of the sample in a magnetic field. At high temperatures above the Néel temperature ($T_N > 310$ K), the ZFC and FC magnetization curves merge each other, probably due to local clustering of the spins and spin glassy behavior [22] or to ferromagnetic domain growth [23]. The ZFC and FC magnetizations curves start to differ below 310 K by the application of 500 Oe; this phenomenon can be interpreted in terms of spin-glass transition or freezing of domain wall motion [24].

The ZFC and FC curves increase monotonically on decreasing temperature from 400 K and exhibit a cusp
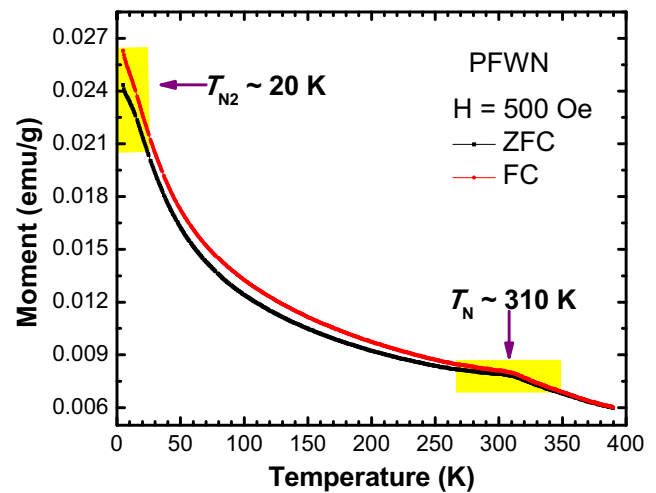

Fig. 4 Temperature dependent molar susceptibility (ZFC and FC) for PFWN at 500 Oe. *Shaded region* shows the 1st and 2nd magnetic phase transition Néel temperature (T_N) and blocking temperature for the spin-glass behavior

around 310 K (T_{N1}), indicating the onset of antiferromagnetic ordering. However, on further decrease in temperature, χ increases further and exhibits another broad hump around 20 K (T_{N2}) before falling rapidly as T approaches to 5 K. This result well supported the reported PFW and PFN results [5, 7, 17]. The Néel temperature (T_N) of the Pb(Fe$_{2/3}$W$_{1/3}$) and Pb(Fe$_{1/2}$Nb$_{1/2}$)O$_3$ $T_N \sim 350$ and 155 K, respectively [5, 6]. The increase in the value of χ starting from 400 K down to 5 K can be attributed to a modified-exchange interaction of Fe^{3+}–O–Fe^{3+} in the disordered regions of the sample like PFW and PFN [5, 6, 23]. Furthermore, the formation of the disordered regions might be due to the synthesis methods adopted, where the grain growth occurs with lattice strain/stress in the material which affects the T_N. The magnetic susceptibility behavior is similar to the earlier Pb-based reports [7, 17, 23, 25, 27].

The observed T_{N1} at 310 K is paramagnetic to antiferromagnetic phase transition. The lower value of the T_{N2} can be attributed to the fluctuations in the local ordering of Fe, Nb, and W ions. Generally, in the well-known perovskite PFW and PFN, antiferromagnetic interactions (T_{N1}) through –Fe^{3+}–O–Fe^{3+}-superexchange paths and –Fe^{3+}–O–Nb–W–O–Fe^{3+}-super-super-exchange paths (T_{N2}) have been both observed. The peak around 20 K in the ZFC curve can be interpreted in terms of spin-glass transition or freezing of domain wall motion [24, 25]. The ZFC-FC bifurcation also exhibits local clustering of the spins [22, 26] or super-antiferromagnetic domain growth [23, 27]. This can also be the source of weak ferromagnetic ordering in the PFWN ceramic. Recently, our group and Chillal et al.'s reported [5, 7, 25] similar behavior on PFN and PFW; two types of magnetic order emerge independently: (i) infinite-range percolation cluster (antiferromagnetic order) and (ii) (Fe^{3+}

ions unblocked) super-antiferromagnetic Fe^{3+} clusters. The coexistence of both the above systems leads to a single homogenous phase, with the magnetic moments arranged in a speromagnetic-like or spin-glass-like fashion. We confirm existence of similar magnetic ordering in this ceramic. This speromagnetic-like behavior is responsible for the existing weak ferromagnetic ordering at RT in our sample. Furthermore, the decrease in χ in the ZFC curves could be a result of the super-antiferromagnetic blocking of the local super-paramagnetic-like clusters present in the sample, confirming the presence of magnetic clusters in the sample having spin glass nature.

It is important to observe the magnetic anomaly at $\sim$ 200–250 K, the ferroelectric ordering temperature (T_C) of PFWN ceramics through the nonlinear behavior of ZFC and FC. The Mössbauer results further supports the presence of these two types of magnetic clustering due to compositional disorder (next section). This kind of magnetic interaction is common in complex-structured lead-based systems, where the B site is occupied by a magnetic and a nonmagnetic cation. According to earlier reports, compounds with good compositional ordering, such as $Pb(Co_{1/2}W_{1/2})O_3$, shows a single magnetic ordering temperature (T_N) at 8 K [28]. However, for $Pb(Fe_{1/2}Nb_{1/2})O_3$ [29, 30] and $Pb(Fe_{1/2}Ta_{1/2})O_3$ [29, 31, 32], where a complete compositional ordering could not be achieved, two magnetic phase transition temperatures ($T_{N1} \sim 161$ K and $T_{N2} \sim 9$ K for $Pb(Fe_{1/2}Nb_{1/2})O_3$ and, $T_{N1} \sim 143$ K and $T_{N2} \sim 9$ K for $Pb(Fe_{1/2}Ta_{1/2})O_3$) have been shown, suggesting the presence of disordered and ordered nanostructures.

From the $M - H$ loop of our PFWN sample in Fig. 5, it can be observed that the magnetization displays a small hysteresis only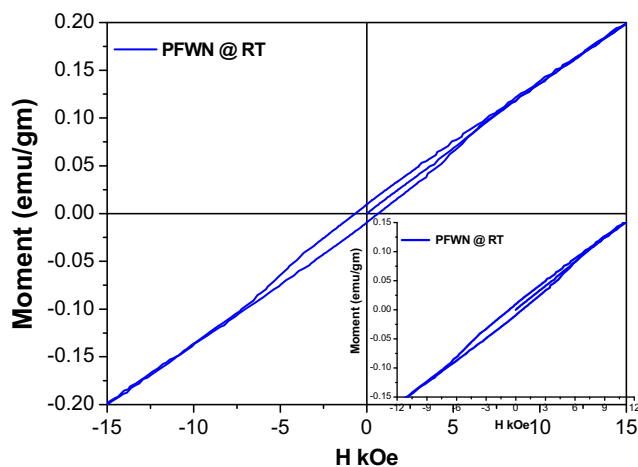 in the low-field region. The appreciable opening of the hysteresis loop reveals the presence of weak ferromagnetism in our sample with a coercive field (H_c) value of 0.768 kOe. The inset in Fig. 5 shows the zoomed in view of the $M - H$ loop around the origin for clarity. The saturated magnetization (M_s) and remnant magnetization (M_r) were estimated to be 1.028 and 0.0095 emu g^{-1}, respectively. For higher applied magnetic fields, the magnetization increases linearly. This paramagnetic-like linear increase of the magnetization at the high field region can be assigned to the weakening of the super-exchange interaction of Fe^{3+}–O–W/Nb–O–Fe^{3+}, caused by the local disorder/short-range order of the Fe atoms at the B site.

3.3 Mössbauer Spectroscopic Studies

The Mössbauer spectrum (Fig. 6) of the PFWN sample measured at RT was fit with a distribution of magnetic hyperfine fields, $P(B_{hf})$. The hyperfine field distribution is shown on the right-hand side of Fig. 6. The obtained average isomer shift (IS) of 0.2030 ± 0.005 mm s^{-1} and quadruple splitting (QS) of 0.4450 ± 0.005 mm s^{-1} corresponds to the Fe^{3+} ions in an octahedral environment [25, 33]. The average magnetic hyperfine field is $\sim 13.54 \pm 1.0$ T. The broad hyperfine field distribution, $P(Bhf)$, indicates that the environments of the Fe ions are not the same, i.e., perfect compositional ordering is not achieved in the studied sample. The Mössbauer spectra is not perfectly sextet; it shows the origin of magnetic behavior due to the near RT T_N (310 K). Recently, Raevskii et al. [33] reported for Pb-based systems where they fit the $P(B_{hf})$ spectrum with a superposition of two sextets and a central (paramagnetic) doublet. From the $P(B_{hf})$ of our sample, it is also clear that along with the broad magnetic hyperfine field distribution, there exists a paramagnetic part. Venevtsev et al. [34] discussed a similar spectrum consisting of two sextets observed after firing the PFW ceramics in oxygen, while the spectrum consists of a single sextet for a sample fired in air. It shows that the existence of a single sextet was due to a fully disordered arrangement of Fe^{3+} ions, while the two sextets in a Mössbauer spectrum for PFWN was associated with a partial disordering of Fe^{3+}, Nb^{5+}, and W^{6+} ions. The formation of two magnetic subsystems might be due to nonequivalent surrounding of iron ions in partially ordered and disordered regions.

Our results well supports to the existence of a partial disordering in our sample which gives rise to the broad hyperfine field distribution, $P(B_{hf})$. Our Mössbauer results well supports the existence of weakly paramagnetic ordering along with antiferromagnetic ordering. This component might be associated with such clusters in the sample where the degree of ordering is higher than the volume average. The results confirmed that there are regions where

Fig. 5 Magnetization of PFWN measured as a function of varying magnetic field at RT. *Inset* shows the enlargement (around the origin) view for clarity

Fig. 6 Room temperature Mössbauer spectrum of PFWN sample. The *figure at the right-hand side* shows the hyperfine field distribution, $P(B_{hf})$
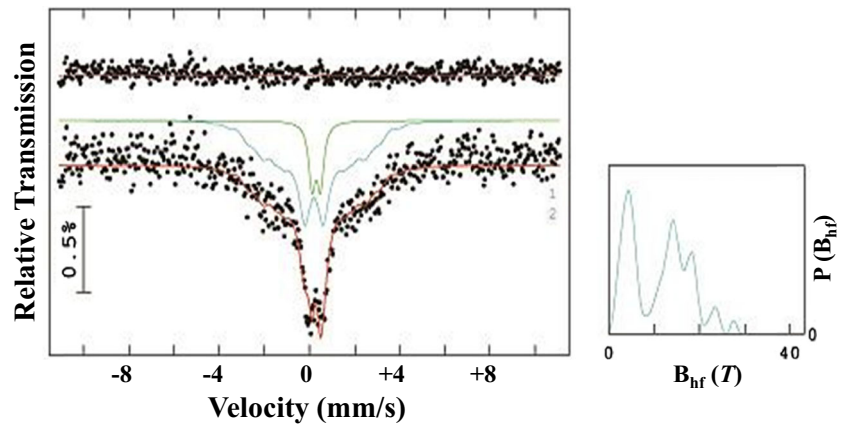
the Fe atoms are compositionally disordered. This disordering breaks the antiferromagnetic ordering of PFWN and shows the RT weak ferromagnetism as observed in the magnetization studies (Section 3.2).

3.4 Ferroelectric ($P - E$ Loops) Studies

Figure 7 shows that the RT ferroelectric properties of the PFWN were investigated by the $P - E$ loop measurement at 50 Hz. In general, PFW does not give a perfect $P - E$ loop at RT due to the high leakage current and T_C. In this synthesis method, sintering was done at 850 °C 1 h^{-1}. This indicates clearly that ceramic pellet was not highly dense due to the low-temperature annealing process. At a maximum applied electric field of ± 2 kV cm^{-1}, the remanent polarization (P_r) is 1.18 μC cm^{-2} and coercive field (E_c) is 1.33 kV cm^{-1}. This clearly indicates that the observed P-E loop, due to the leakage current in the sample and also the low P_r value in
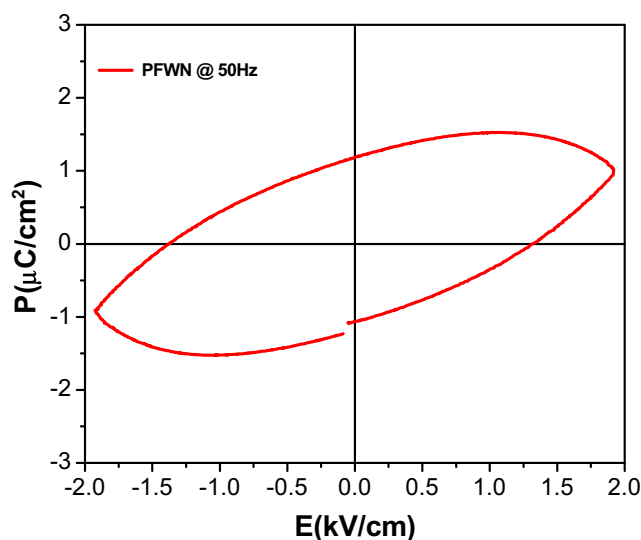
the sample are due to the combined effect of the crystalline lattice structure, defects, oxygen vacancies, and the stoichiometry. In addition, the E_c also shows noticeable values; this can be attributed to crystallite sizes, interface, and the defects of the sample. The asymmetry of the $P - E$ loop can be attributed primarily to the difference in the work function, the crystallographic defect distribution, and the thermal history between the top and the bottom electrodes [35]. The ferroelectric ordering may be there, but the effect is too low in the sample; one has to study the low-temperature P–E loops to understand the detailed mechanism.

From the RT ND results, we have not confirmed existence of ferromagnetic ordering. But, magnetic studies show a clear opening of M–H (hysteresis) loop (Section 3.2), justifying the presence of weak ferromagnetism. Hence, from the leakage current-based $P - E$ loops, it is clear that the weak ferromagnetism observed in the M–H loop of the antiferromagnetic PFWN sample, at RT, originates from the defected, nonstoichiometric, or disordered regions and is isolated from the perfect antiferromagnetism of the PFWN sample.

4 Conclusions

In conclusion, PFWN multiferroic ceramics were synthesized at relatively low calcination and sintering temperatures by a Columbite solid-state reaction method followed by closed environment technique. The RT XRD and ND studies showed that PFWN is in the *cubic* phase with *Pm-3m* space group. The ND data confirms the presence of G-type antiferromagnetic structure. The ND and Mössbauer spectroscopy results confirm the iron in the sample is in the Fe^{3+} (high spin) state. It further suggests that iron, tungsten, and niobium atoms are randomly distributed at the available octahedral sites which evidenced the compositional disorder. The existence of weak ferromagnetic ordering in the

Fig. 7 Room temperature $P - E$ loops measured at 50 Hz

sample is confirmed by the $M-H$ loop results, and it is well supported by the RT Mössbauer spectroscopy.

The temperature-dependent magnetic susceptibility (χ vs. T) of PFWN possesses two inflexion points; one at $\sim$ 310 K corresponding to the Néel temperature (T_{N1}) and another at $\sim$ 20 K (T_{N2}) corresponding to a spin-glass-like transition. The RT weak ferromagnetism, spin glass, and anti-ferromagnetic ordering at $\sim$ 310 K result suggest that the existence of long-ranged AFM and ferromagnetism originates from different regions in the sample. But, the weak ferromagnetism originates from the local uncompensated spins of the compositionally disordered Fe ions and χ vs. T results corroborate the above conclusion. Finally, ferroelectric hysteresis loops at RT confirm the presence of weak ferroelectric behavior. This material can be used for future RT magnetoelectric multiferroics.

References

1. Aizu, K.: Possible species of ferromagnetic, ferroelectric, and ferroelastic crystals. Phys. Rev. B **2**, 754–772 (1970)
2. Toledano, J.C.: Ferroelasticity. Ann. Telecommun **29**, 249–27 (1974)
3. Schmid, H., Trooster, J.M.: Mossbauer effect and optical evidence for new phase transitions in Fe-Cl, Fe-Br, Fe-I, Co-Cl and Zn-Cl boracite. Sol. St. Commun. **5**, 31–35 (1967)
4. Smolenskii, G.A.: Usp. Fiz. Nauk. **137**, 415–448 (1982)
5. Matteppanavar, S., Rayaprol, S., Anupama, A.V., Angadi, B., Sahoo, B.: Origin of RT weak-ferromagnetism in antiferromagnetic Pb(Fe$_{2/3}$W$_{1/3}$)O$_3$ ceramic. Ceram. Int. **41**(9), 11680–11686 (2015)
6. Matteppanavar, S., Rayaprol, S., Singh, K., Reddy, V.R., Angadi, B.: Evidence for magneto-electric and spin–lattice coupling in PbFe$_{0.5}$Nb$_{0.5}$O$_3$ through structural and magneto-electric studies. J. Mater. Sci. **50**, 4980–4993 (2015)
7. Matteppanavar, S., Rayaprol, S., Anupama, A.V., Angadi, B., Sahoo, B.: On the RT ferromagnetic and ferroelectric properties of Pb(Fe$_{1/2}$Nb$_{1/2}$)O$_3$. J. Supercond. Nov. Magn. **28**(8), 2465–2472 (2015)
8. Kumar, A.R., Katiyar, S., Premnath, R.M., Rinaldi, C., Scott, J.F.: Strain-induced artificial multiferroicity in Pb(Zr$_{0.53}$Ti$_{0.47}$)O$_3$/Pb(Fe$_{0.66}$W$_{0.33}$)O$_3$ layered nanostructure at ambient temperature. J. Mater. Sci. **44**, 5113 (2009)
9. Daesu, L., Sang, M.Y., Younghun, J., Song, T.K.: Room-temperature multiferroic properties of Pb(Zr$_{0.57}$Ti$_{0.43}$)O$_3$–Pb(Fe$_{0.67}$W$_{0.33}$)O$_3$ solid-solution epitaxial thin films. Kor. Phy. Soc. **57**(6), 1914–1918 (2010)
10. Kempa, M., Kamba, S., Savinov, M., Marysko, M., Frait, Z., Vanek, P., Tomczyk, M., Vilarinho, P.M.: Bulk dielectric and magnetic properties of PFW–PZT ceramics: absence of magnetically switched-off polarization. J. Phys.: Condens. Matter **22**, 445902 (2010)
11. Pajic, D., Jagodic, M., Jaglicic, Z., Holc, J., Kosec, M., Trontelj, Z.: Competing antiferromagnetism and local magnetic order in the bulk ceramic PZT–PFW multiferroic system: searching for the most promising ratio between PZT and PFW. J. Phys. D: Appl. Phys. **46**, 455001 (2013)
12. Dulkin, E., Mojaev, E., Roth, M., Kamba, S., Vilarinho, P.M.: Burns, Néel, and structural phase transitions in multiferroic Pb(Fe$_{2/3}$W$_{1/3}$)O$_3$–xPbTiO$_3$ detected by an acoustic emission. J. Appl. Phys. **103**, 083542 (2008)
13. Choudhary, R.N.P., Pradhan, D.K., Tirado, C.M., Bonilla, G.E., Katiyar, R.S.: Relaxor characteristics of Pb(Fe$_{2/3}$W$_{1/3}$)O$_3$–BiFeO$_3$ solid solution prepared by mechanosynthesis route. J. Appl. Phys. **100**, 084105 (2006)
14. Puli, V.S., Martnez, R.V., Kumar, A., Scott, J.F., Katiyar, R.S.: A quaternary lead based perovskite structured materials with diffuse phase transition behavior. Mater. Res. Bul **46**, 2527–2530 (2011)
15. Lee, B.H., Kim, N.K., Kim, J.J., Cho, S.H.: Ferroelecrrics **211**, 233–247 (1998)
16. Liou, Y.C., Shih, Y.C., Chuang, C.J.: PZN-PFW and PFN-PFW relaxor ferroelectric ceramics by a reaction-sintering process. J. Electroceram. **13**, 457–46 (2004)
17. Ivanova, S.A., Eriksson, S.-G., Tellgren, R., Rundlof, H.: Neutron powder diffraction study of the magnetoelectric relaxor Pb(Fe$_{2/3}$W$_{1/3}$)O$_3$. Mater. Res. Bul. **39**, 2317–2328 (2004)
18. Matteppanavar, S., Angadi, B., Rayaprol, S.: Neutron diffraction studies on chemical and magnetic structure of multiferroic PbFe$_{0.67}$W$_{0.33}$O$_3$. AIP Conf. Proc. **1591**, 1669–1671 (2014)
19. Singh, M.K., Katiyar, R.S., Scott, J.F.: New magnetic phase transitions in BiFeO$_3$. J. Phys. Condens. Matter **20**, 252203 (2008)
20. Brand, R.A.: Nucl. Instrum. Methods B **28**, 398 (1987)
21. Rodriguez-Carvajal, J.: BASIREPS: A program for calculating irreducible representations of space groups and basis functions for axial and polar vector properties (2007)
22. Havlicek, R., Vejpravova, J.P., Bochenek, D.: Structure and magnetic properties of perovskite-like multiferroic PbFe$_{0.5}$Nb$_{0.5}$O$_3$. J. Phys. Conf. Ser **0120581** (2010)
23. Vincent, E., Dupuis, V., Alba, M., Hammann, J., Bouchaud, J.P.: Aging phenomena in spin-glass and ferromagnetic phases: domain growth and wall dynamics. Europhys. Lett. **50**, 674 (2000)
24. Chang, H., Guo, Y.Q., Liang, J.K., Rao, G.H.: J. Magn. Magn. Mater **278**, 306 (2004)
25. Chillal, S., Thede, M., Litterst, F.J., Gvasaliya, S.N., Shaplygina, T.A., Lushnikov, S.G., Zheludev, A.: Microscopic coexistence of antiferromagnetic and spin-glass states. Phys. Rev. B **87**, 220403(R)–220406 (2013)
26. Kleemann, W., Shvartsman, V.V., Borisov, P.: Coexistence of antiferromagnetic and spin cluster glass order in the magnetoelectric relaxor multiferroic Pb(Fe$_{1/2}$Nb$_{1/2}$)O$_3$. Phys. Rev. Lett. **105**, 257202 (2010)
27. Laguta, V.V., Rosa, J., Jastrabik, L., Blinc, R., Cevc, P., Zalar, B., Remskar, M., Raevskaya, S.I., Raevski, I.P.: IP, ^{93}Nb NMR and Fe^{3+} EPR study of local magnetic properties of magnetoelectric Pb(Fe$_{1/2}$Nb$_{1/2}$)O$_3$. Mater. Res. Bull. **45**, 1720 (2010)
28. Astrov, D.N., Alshin, B.I., Zorin, R.V., Drobyshev, L.A.: In: J. F. Allen (ed.) Proc. 11th International Conference on Low Temperature Physics (1968), vol. 2 (1969)
29. Astrov, D.N., Alshin, B.I., Zorin, R.V., Drobyshev, L.A.: Spontaneous magnetoelectric effect. Sov. Phys.-JETP **55**, 2122–2127 (1968)

30. Brixel, W., Rivera, J.P., Steiner, A., Schmid, H.: Magnetic field induced magnetoelectric effects, (ME)H, in the perovskites Pb_2CoWO_6 and Pb_2FeTaO_6. Ferroelectrics **79**, 201–204 (1988)

31. Kiselev, S.V., Ozerov, R.P.: Soviet Phys.-Solid State **11**, 1133 (1969)

32. Nomura, S., Takabayashi, H., Nakagawa, T.: Dielectric and magnetic properties of $Pb(Fe_{1/2}Ta_{1/2})O_3$. Jpn. J. Appl. Phys. **7**, 600 (1968)

33. Raevskii, I.P., Sarychev, D.A., Bryugeman, S.A., Reznichenko, L.A., Shilkina, L.A., Razumovskaya, O.N., Nikolaev, V.S., Vyshatko, N.P., Salak, A.N.: Study of cation ordering and magnetic phase transitions in ternary Fe-containing perovskite oxides by Mössbauer spectroscopy. Crystallograph. Reports **47**(6), 1012–1015 (2002). Translated from Kristallografiya **47**(6), 1081–1084 (2002)

34. Venevtsev, Y.u.N., Sklyarevskiĭ, V.V., Lukashevich, I.I.: Kristallografiya **21**(5), 971 (1976). [Sov. Phys. Crystallogr. **21**, 556 (1976)]

35. Lee, Y.H., Wu, J.M., Chueh, Y., Chou, L.J.: Low-temperature growth and interface characterization of BiFeO3 thin films with reduced leakage current. Appl. Phys. Lett. **87**, 17290 (2005)